Coupled CH_4 production and oxidation support CO_2 supersaturation in a tropical flood pulse lake (Tonle Sap Lake, Cambodia)

Benjamin Lloyd Miller[a,b,1], Gordon William Holtgrieve[a], Mauricio Eduardo Arias[c], Sophorn Uy[d,e], and Phen Chheng[f]

[a]School of Aquatic and Fishery Sciences, University of Washington, Seattle, WA 98105; [b]School of Environmental and Forest Sciences, University of Washington, Seattle, WA 98195; [c]Department of Civil and Environmental Engineering, University of South Florida, Tampa, FL 33620; [d]Inland Fisheries Research and Development Institute, Phnom Penh, Cambodia; [e]Faculty of Fisheries, Royal University of Agriculture, Phnom Penh, Cambodia; and [f]Fisheries Administration, Phnom Penh, Cambodia

Edited by Peter Raymond, Yale University, New Haven, CT; received April 22, 2021; accepted December 8, 2021 by Editorial Board Member Mary E. Power

Carbon dioxide (CO_2) supersaturation in lakes and rivers worldwide is commonly attributed to terrestrial–aquatic transfers of organic and inorganic carbon (C) and subsequent, in situ aerobic respiration. Methane (CH_4) production and oxidation also contribute CO_2 to freshwaters, yet this remains largely unquantified. Flood pulse lakes and rivers in the tropics are hypothesized to receive large inputs of dissolved CO_2 and CH_4 from floodplains characterized by hypoxia and reducing conditions. We measured stable C isotopes of CO_2 and CH_4, aerobic respiration, and CH_4 production and oxidation during two flood stages in Tonle Sap Lake (Cambodia) to determine whether dissolved CO_2 in this tropical flood pulse ecosystem has a methanogenic origin. Mean CO_2 supersaturation of 11,000 ± 9,000 μatm could not be explained by aerobic respiration alone. ^{13}C depletion of dissolved CO_2 relative to other sources of organic and inorganic C, together with corresponding ^{13}C enrichment of CH_4, suggested extensive CH_4 oxidation. A stable isotope-mixing model shows that the oxidation of ^{13}C depleted CH_4 to CO_2 contributes between 47 and 67% of dissolved CO_2 in Tonle Sap Lake. ^{13}C depletion of dissolved CO_2 was correlated to independently measured rates of CH_4 production and oxidation within the water column and underlying lake sediments. However, mass balance indicates that most of this CH_4 production and oxidation occurs elsewhere, within inundated soils and other floodplain habitats. Seasonal inundation of floodplains is a common feature of tropical freshwaters, where high reported CO_2 supersaturation and atmospheric emissions may be explained in part by coupled CH_4 production and oxidation.

carbon dioxide supersaturation | methane oxidation | flood pulse | lake

Globally, most lakes and rivers are supersaturated with dissolved carbon dioxide (CO_2) relative to the atmosphere, highlighting their outsized role in transferring and transforming terrestrial carbon (C) (1–3). Terrestrial–aquatic transfers of C can include CO_2 dissolved in terrestrial ground and surface waters (3–6), dissolved inorganic carbon (DIC) from carbonate weathering (7, 8), or organic C from various sources that is subsequently respired in lakes and rivers (9, 10). Initially, oceanic export was thought to be the only fate for terrestrial–aquatic transfers of C, but a growing body of research on sediment burial of organic C and CO_2 emissions from freshwaters prompted the "active pipe" revision to this initial set of assumptions (11). Although freshwaters are now recognized as focal points for transferring and transforming C on the landscape, most of this research has been conducted within temperate freshwaters (2, 11, 12). Few studies focus on the mechanisms of CO_2 supersaturation in tropical lakes and rivers, with most conducted in just one watershed, the Amazon (4, 13–15).

CO_2 supersaturation within tropical freshwaters is likely influenced by their unique flood pulse hydrology. The canonical flood pulse concept hypothesizes that annual flooding of riparian land will lead to organic C mobilization and respiration (16). Partial pressures of CO_2 (pCO_2) have been measured in excess of 44,000 μatm in the Amazon River (13), 16,000 μatm in the Congo River (17), and 12,000 μatm in the Lukulu River (17). Richey et al. (13), Borges et al. (18), and Zuidgeest et al. (17) have each shown that that riverine pCO_2 scales with the amount of land flooded in these watersheds. Yet it was only recently that Abril and Borges (19) proposed the importance of flooded land to the "active pipe." These authors differentiate uplands that unidirectionally drain water downhill (via ground and surface water) from floodplains that bidirectionally exchange water with lakes and rivers (19). They conceptualize how floodplains combine high hydrologic connectivity, high rates of primary production, and high rates of respiration to transfer relatively large amounts of C to tropical freshwaters (19).

Methanogenesis inevitably results on floodplains after dissolved oxygen (O_2) and other electron acceptors for anaerobic respiration such as iron and sulfate are consumed (16, 19). Horizontal gradients in dissolved O_2 and reducing conditions have been observed extending from the center of lakes and rivers through their floodplains in the Mekong (20, 21),

Significance

Freshwaters inextricably link flows of carbon between the land, oceans, and atmosphere. Resulting carbon dioxide supersaturation relative to the atmosphere in most of the world's lakes and rivers has long been assumed to come from aerobic respiration. Although carbon dioxide also comes from the oxidation of anaerobically produced methane, this has been largely ignored within freshwaters. Here, we use stable carbon isotopes of carbon dioxide and methane to show that a nontrivial proportion of the total dissolved carbon dioxide in a tropical flood pulse lake comes from methane oxidation. Seasonal pulses of flooding are common in the tropics, suggesting that coupled methane production and oxidation likely contribute more broadly to flows of carbon between the land, understudied tropical freshwaters, and atmosphere.

Author contributions: B.L.M., G.W.H., M.E.A., and P.C. designed research; B.L.M. and S.U. performed research; B.L.M., G.W.H., and M.E.A. contributed new analytic tools; B.L.M. analyzed data; and B.L.M. and G.W.H. wrote the paper.

The authors declare no competing interest.

This article is a PNAS Direct Submission. P.R. is a guest editor invited by the Editorial Board.

[1]To whom correspondence may be addressed. Email: blm8@uw.edu.

This article contains supporting information online at http://www.pnas.org/lookup/suppl/doi:10.1073/pnas.2107667119/-/DCSupplemental.

Published February 14, 2022.

Table 1. Mean partial pressures (μatm) ± 1 SD and δ^{13}C () ± 1 SD for CO_2 and CH_4 in open water, edge, and floodplain environments of TSL during the high-water and falling-water stages of the flood pulse

	pCO_2 (μ atm)	pCH_4 (μ atm)	δ^{13}C-CO_2 (‰)	δ^{13}C-CH_4 (‰) n	n
High					
All environments	13,000 ± 6,000	11,000 ± 2,000	−40 ± 7	−36 ± 2	35
Open	12,000 ± 4,000	3,000 ± 2,000	−37 ± 4	−45 ± 9	6
Edge	14,000 ± 6,000	20,000 ± 10,000	−39 ± 6	−38 ± 6	6
Floodplain	13000 ± 6,000	11,000 ± 2,000	−41 ± 7	−34 ± 2	23
Falling					
All environments	13,000 ± 12,000	600 ± 300	−38 ± 5	−62 ± 5	12
Open	14,000 ± 13,000	50 ± 20	−35 ± 3	−57 ± 6	6
Edge	14,000 ± 12,000	1,400 ± 800	−40 ± 6	−67 ± 7	6

Mean partial pressures (μ atm) and δ^{13}C (‰) across all lake environments for the high-water and falling-water stages are also shown.

Congo (22), Pantanal (23), and Amazon watersheds (4). CH_4 production and oxidation occur along such redox gradients (4, 16, 19, 23). CH_4 is produced by acetate fermentation (Eq. **1**) and carbonate reduction (Eq. **2**) within freshwaters (24, 25). CH_4 production coupled with aerobic oxidation results in CO_2 (Eq. **3** and ref. 25), yet no studies have quantified the relative contribution of coupled CH_4 production and oxidation to CO_2 supersaturation within tropical freshwaters.

$$CH_3COOH \rightarrow CO_2 + CH_4, \quad [1]$$

$$CO_2 + 8H^+ + 8e^- \rightarrow CH_4 + 2H_2O, \quad [2]$$

$$CH_4 + 2O_2 \rightarrow CO_2 + 2H_2O. \quad [3]$$

The relative contribution of coupled CH_4 production and oxidation to CO_2 supersaturation within tropical freshwaters can be traced with stable C isotopes of CO_2 and CH_4. Methanogenesis results in CH_4 that is depleted in ^{13}C ($\delta^{13}C = -65$ to -50‰ from acetate fermentation and -110 to -60‰ from carbonate reduction) compared to other potential sources of organic and inorganic C ($\delta^{13}C = -37$ to -7.7‰; see *Materials and Methods*) (24–26). The oxidation of this ^{13}C-depleted CH_4 results in ^{13}C-depleted CO_2 (24–26). At the same time, CH_4 oxidation enriches the $^{13}C/^{12}C$ of residual CH_4 as bacteria and archaea preferentially oxidize ^{12}C-CH_4 (25). This means that the $^{13}C/^{12}C$ of CO_2 and CH_4 can serve as powerful tools to determine the source of CO_2 supersaturation within freshwaters.

Tonle Sap Lake (TSL) is Southeast Asia's largest lake and an understudied flood pulse ecosystem that supports a regionally important fishery (21, 22, 27). Each May through October, monsoonal rains and Himalayan snowmelt increase discharge in the Mekong River and cause one of its tributaries, the Tonle Sap River, to reverse course from southeast to northwest (21). During this course reversal, the Tonle Sap River floods TSL. The TSL flood pulse increases lake volume from 1.6 to 60 km^3 and inundates 12,000 km^2 of floodplain for 3 to 6 mo per year (21, 27). Holtgrieve et al. (22) have shown that aerobic respiration is consistently greater than primary production in TSL (i.e., net heterotrophy), with the expectation of consistent CO_2 supersaturation. But, the partial pressures, C isotopic compositions, and ultimately the source of dissolved CO_2 in TSL remain unquantified.

To quantify CO_2 supersaturation and its origins in TSL, we measured the partial pressures of CO_2 and CH_4 and compared their C isotopic composition to other potential sources of organic and inorganic C. We carried out these measurements in distinct lake environments during the high-water and falling-water stages of the flood pulse, hypothesizing that CH_4 production and oxidation on the TSL floodplain would support CO_2 supersaturation during the high-water stage. We found that coupled CH_4 production and oxidation account for a nontrivial proportion of the total dissolved CO_2 in all TSL environments and during both flood stages, showing that anaerobic degradation of organic C at aquatic–terrestrial transitions can support CO_2 supersaturation within tropical freshwaters.

Results

pCO_2 and pCH_4 in TSL were consistently supersaturated relative to atmospheric equilibrium. pCO_2 averaged 13,000 ± 6,000 μatm (mean ± 1 SD) across sites during the high-water stage and 13,000 ± 12,000 μatm during the falling-water stage (Table 1). pCH_4 was significantly greater during the high-water stage (11,000 ± 2,000 μ atm) than during the falling-water stage (600 ± 300 μ atm) ($P < 0.001$, $d = 1.8$). By contrast, pCO_2 and pCH_4 at sea level are ∼400 and 1.8 μ atm, respectively.

CO_2 supersaturation exceeded dissolved O_2 deficits, indicating sources of dissolved CO_2 other than aerobic respiration (Fig. 1 *A* and *B*). CO_2 supersaturation is expected to vary with dissolved O_2 deficits in a $-1/1$ O_2:CO_2 ratio as one μ micromole of dissolved O_2 is consumed for each μ micromole of dissolved CO_2 produced. Instead, ratios of $-0.1/1$ were observed during both the high-water and falling-water stages. During the high-water stage, the greatest CO_2 supersaturation occurred under the most hypoxic conditions (Fig. 1*A*).

The intercept of the relationship between $1/CO_2$ and δ^{13}C-CO_2 can be used to determine the source of dissolved CO_2 (Keeling Intercepts; *SI Appendix*, Table S1) (28, 29). In TSL, the inverse of pCO_2 was strongly correlated with ^{13}C depletion of CO_2. The intercept of δ^{13}C-CO_2 was as low as -51‰ during the high-water stage and -43‰ during the falling-water stage. This indicates a ^{13}C-depleted source of dissolved CO_2 relative to the other potential sources of organic and inorganic C measured, which ranged from -37 to -7.7‰ (Fig. 2*A*). Observed ^{13}C depletion of dissolved CO_2 coincided with ^{13}C enrichment of dissolved CH_4 (Table 1 and Fig. 3 *A* and *B*). Acetate fermentation produces δ^{13}C-CH_4 ranging from -65 to -50‰ and carbonate reduction produces δ^{13}C-CH_4 ranging from -110 to -60‰ (24–26). By contrast, δ^{13}C-CH_4 averaged -36 ± 2‰ during the high-water stage. During this flood stage, dissolved CO_2 became more ^{13}C depleted, and dissolved CH_4 became more ^{13}C enriched from open water environments (δ^{13}C-CO_2 = -37 ± 4‰, δ^{13}C-CH_4 = -45 ± 9‰) to edge environments (δ^{13}C-CO_2 = -39 ± 6‰, δ^{13}C-CH_4 = -38 ± 6‰) to floodplain environments (δ^{13}C-CO_2 = -41 ± 7‰, δ^{13}C-CH_4 = -34 ± 2‰). Net fractionation between δ^{13}C-CO_2 and δ^{13}C-CH_4 (simply, δ^{13}C-CO_2 – δ^{13}C-CH_4) of typically <10‰ in TSL indicates substantial CH_4 oxidation (25) (Fig. 3 *A* and *B*).

A two-source, stable isotope-mixing model for δ^{13}C-CO_2 was used to estimate fractional contributions to dissolved CO_2 by CH_4 oxidation, compared with other potential sources of organic and inorganic C (Fig. 2*A*). Assuming oxidation of CH_4

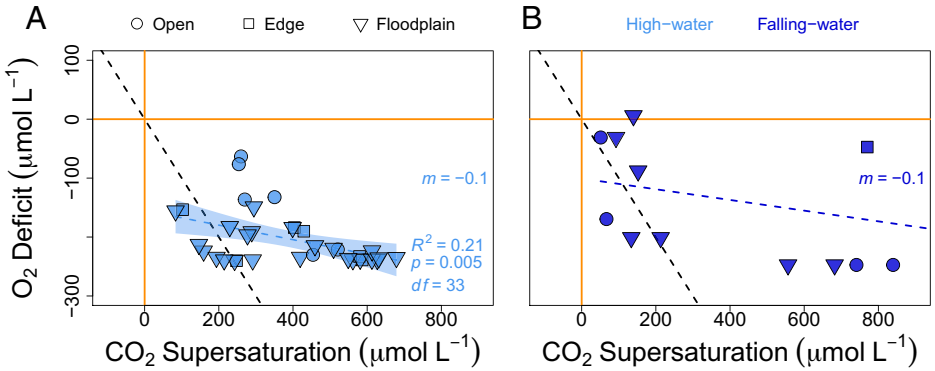

Fig. 1. Dissolved O_2 deficit and CO_2 supersaturation, relative to atmospheric equilibrium in open water, edge, and floodplain environments of TSL (*A*) during the high-water and falling-water stages of the flood pulse (*B*). Dissolved O_2 deficit and CO_2 supersaturation are calculated as the difference between atmospheric equilibrium, according to Henry's Law. Orange lines show atmospheric equilibrium at a dissolved O_2 deficit and CO_2 supersaturation of 0 μ mol $\cdot$ L^{-1}. A slope (*m*) of −1.0 represents the equimolar consumption of dissolved O_2 and production of dissolved CO_2 expected during aerobic respiration (black dashed line). Instead, a slope of −0.1 was observed during both the high-water and falling-water stages. O_2 deficits were strongly correlated to CO_2 supersaturation during the high-water stage, but there was no such correlation during the falling-water stage.

produced by acetate fermentation only, the fractional contributions by CH_4 oxidation to dissolved CO_2 range from 63 to 85% across the distinct lake environments and flood stages of TSL (*SI Appendix*, Table S3). Assuming oxidation of CH_4 produced by both acetate fermentation and carbonate reduction, these contributions by CH_4 oxidation fall to a more conservative 47 to 67%. Apparent fractionation between δ^{13}C-CO_2 and δ^{13}C-CH_4 (simply, δ^{13}C-CO_2/δ^{13}C-CH_4) of typically <1.055 in TSL indicate substantial CH_4 production by acetate fermentation with some carbonate reduction (24, 25) (Fig. 2*B*).

δ^{13}C-CO_2 was strongly correlated to independent measurements of net CH_4 oxidation in the water column during the high-water stage (Fig. 3 *C* and *D*). The same significant relationship was observed between δ^{13}C-CO_2 and gross CH_4 production within the sediments (Fig. 3 *E* and *F*). Despite these relationships, CO_2 mass balance indicates that CH_4 production and oxidation within the water column and underlying sediments contribute at most 9% to dissolved CO_2 in TSL (*SI Appendix*, Table S4). Of these two processes, CH_4 production contributes one to two orders of magnitude more CO_2 than CH_4 oxidation. Other processing of C within the water column and underlying sediments, such as aerobic respiration, also contribute a relatively small share of total dissolved CO_2 (13 ± 8%).

Discussion

Contributions of CH_4 production and oxidation to CO_2 supersaturation are understudied within tropical freshwaters, where extensive flooding, dissolved O_2 deficits, and reducing conditions at aquatic–terrestrial transitions make such contributions likely. The subtropics and tropics are home to many high-order flood pulse rivers, such as the Amazon, Orinoco, Congo, Zambezi, and Mekong, which are collectively responsible for over 30% of global mean annual discharge (30). Along this tropical "active pipe" lays 52% of the world's floodplains, transferring and transforming C at relatively high rates (20, 31). Using a combination of isotopic tracers and mass balance, we show that a substantial fraction this transfer and transformation of C occurs through coupled CH_4 production and oxidation in TSL.

A majority of our measured δ^{13}C-CO_2 fell between the ^{13}C-depleted CO_2 known to result from CH_4 oxidation and

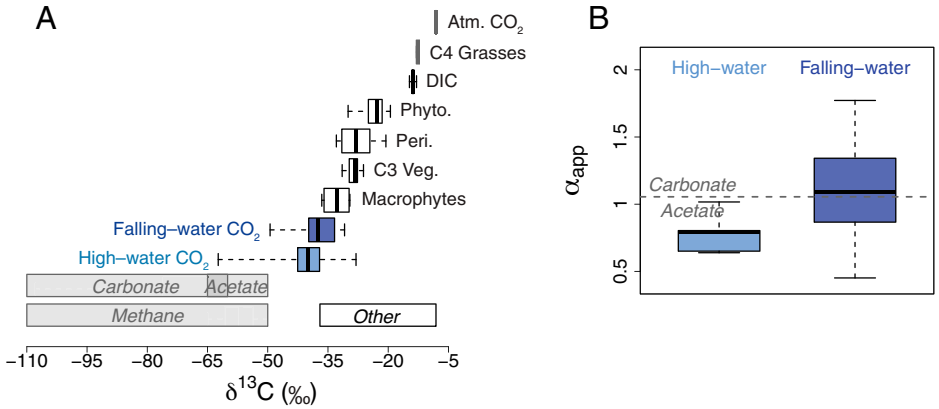

Fig. 2. (*A*) Measured δ^{13}C-CO_2 (blue) relative to other potential sources of organic and inorganic C during the high-water and falling-water stages of the flood pulse. "Other" potential sources of organic and inorganic C measured by this study in TSL include macrophytes, terrestrial C3 vegetation, periphyton, phytoplankton, and DIC. Emergent aquatic C4 grasses, measured by Hedges et al. (48) in the Amazon, and atmospheric CO_2 in equilibrium with water (47) are also included. Isotopic values quantified by this study are in blue and white, and those quantified by other studies (24–26, 47, 48) are in gray. (*B*) Apparent fractionation between δ^{13}C-CO_2 and δ^{13}C-CH_4 (α_{app}) indicated substantial CH_4 production through acetate fermentation with some carbonate reduction in TSL (24, 25). Therefore, a two-source, isotope-mixing model was created using 1) a continuous uniform distribution of δ^{13}C-CO_2 known to result from the oxidation of CH_4 produced by both pathways (gray boxes) and 2) a continuous, uniform distribution of δ^{13}C-CO_2 from DIC and the aerobic respiration of potential organic C sources (white box).

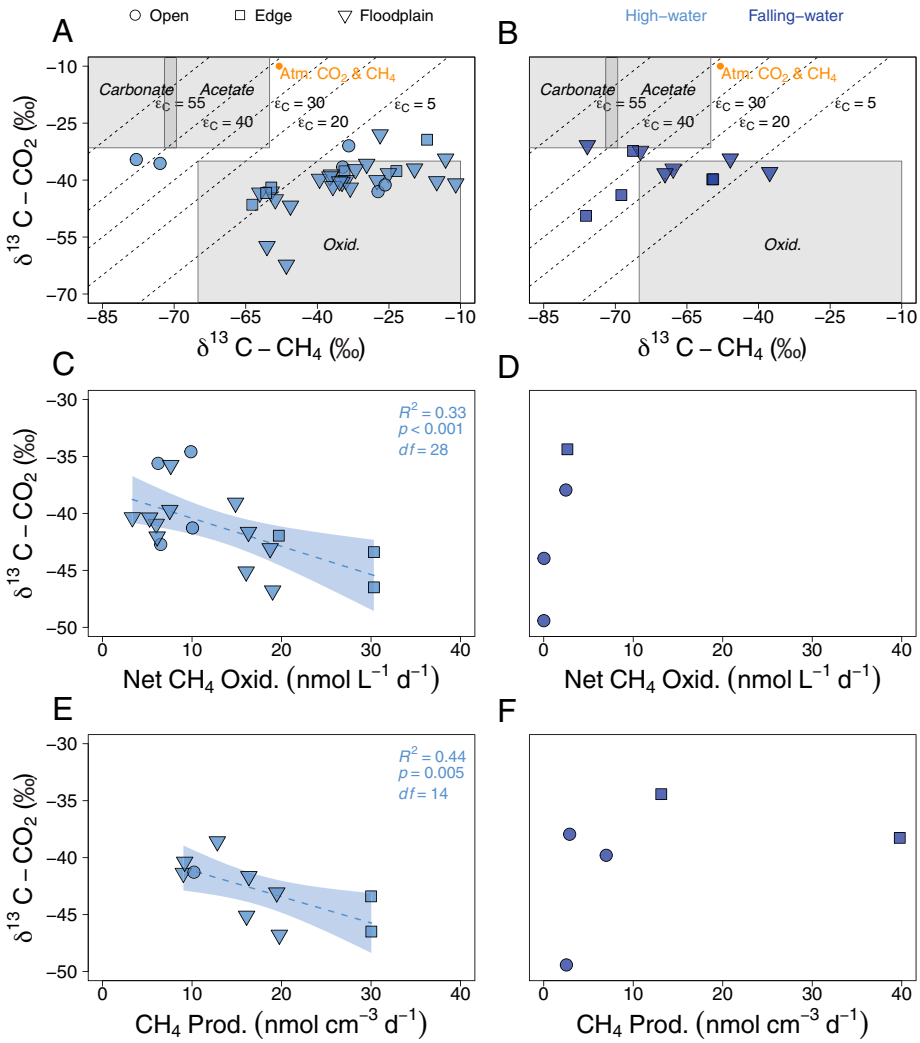

Fig. 3. δ^{13}C-CO_2 and δ^{13}C-CH_4 in open-water, edge, and floodplain environments of TSL during the high-water (*A*) and falling-water stages of the flood pulse, modified from Whiticar (25) (*B*). Zones of CH_4 production by acetate fermentation, CH_4 production by carbonate reduction, and CH_4 oxidation based on apparent fractionation between δ^{13}C-CO_2 and δ^{13}C-CH_4 (ε_C) are shaded in gray. ^{13}C depletion of CO_2 was strongly correlated to independent measurements of net CH_4 oxidation in the water column during the high-water stage (*C*), though not during the falling-water stage (*D*). ^{13}C depletion of CO_2 was also strongly correlated to gross CH_4 production within sediments during the high-water stage (*E*), though not during the falling-water stage (*F*).

the relatively more ^{13}C-enriched phytoplankton, periphyton, macrophytes, and terrestrial C3 vegetation measured in TSL (Fig. 2*A*). Because there is little fractionation during aerobic respiration of organic C, measured δ^{13}C-CO_2 in lakes can be expected to fall inside the range of δ^{13}C observed for commonly considered sources of organic and inorganic C (31, 32). Instead, our observed δ^{13}C-CO_2 fell outside of this range. Potential sources of organic and inorganic C in TSL ranged from $\delta^{13}C = -37‰$ for macrophytes to $\delta^{13}C = -7.7‰$ for atmospheric CO_2 in equilibrium with water. De Kluiver and others (33, 34) have reported relatively ^{13}C-depleted phytoplankton ($\delta^{13}C = -41‰$, *SI Appendix*, Table S2). However, the net heterotrophy and CO_2 supersaturation consistently observed in TSL and other lakes (34) makes substantial contributions to dissolved CO_2 from aquatic primary producers such as phytoplankton unlikely, because these ecosystems are inferred to receive greater inputs of terrestrial organic C than aquatic organic C. Accordingly, the δ^{13}C of dissolved CO_2 measured in the same study by De Kluiver et al. (34) ranges from −21 to −9‰, suggesting that the aerobic respiration of relatively ^{13}C-depleted phytoplankton in net heterotrophic lakes does not substantially impact δ^{13}C-CO_2. Furthermore, our most ^{13}C-depleted dissolved CO_2 was sampled on the TSL floodplain, where the water column and underlying sediments are largely shaded by macrophytes and other emergent vegetation, limiting phytoplankton production (20). Ultimately, methanogenesis is the only possible source of the ^{13}C-depleted, dissolved CO_2 observed in TSL. We can therefore use a two-source, stable isotope-mixing model to estimate relative contributions to dissolved CO_2 by 1) potential sources of organic and inorganic C and 2) CH_4 oxidation. This mixing model shows that CH_4 oxidation contributes between 47 and 67% of dissolved C-CO_2 across the distinct lake environments and flood stages of TSL, which is unprecedented in the aquatic C-cycling literature.

High-CO_2 supersaturation and an imbalance with dissolved O_2 such as we observed in TSL (Fig. 1 *A* and *B*) have previously been attributed to autotrophic and heterotrophic respiration of macrophytes and other emergent aquatic vegetation on flooded land (15, 16, 17, 35). Macrophytes and other emergent aquatic vegetation fix primarily atmospheric CO_2, acting more as terrestrial primary producers than aquatic primary producers. Melack and Engle (35) have shown that floating macrophytes dominate primary production and provide the bulk of organic C to an Amazon floodplain lake. Abril et al. (15) have further suggested that floodplain and riparian wetland

vegetation in the Amazon could export fully half of its primary production on an annual basis. Data from TSL supports a more nuanced interpretation. The most ^{13}C-depleted source of organic C in TSL was an individual macrophyte ($\delta^{13}C = -37‰$, mean $\delta^{13}C = -33 \pm 4‰$). Even so, 70% of our dissolved CO_2 measurements were depleted in ^{13}C below $-37‰$. As confirmed by our stable isotope-mixing model, this means that aerobic respiration of macrophytes can contribute to but not explain the C isotopic depletion of dissolved CO_2 observed in TSL.

Corresponding ^{13}C enrichment of dissolved CH_4 indicated a fractionating loss process, further supporting the interpretation that CH_4 oxidation supports CO_2 supersaturation in TSL. Acetate fermentation within tropical lake sediments from the Amazon and Pantanal has been shown to produce δ^{13}C-CH_4 values ranging from -86 to $-61‰$ (36, 37). The same studies showed concurrent carbonate reduction producing CH_4 even more depleted in ^{13}C (36, 37). By contrast, we measured an overall mean δ^{13}C-CH_4 of $-43 \pm 9‰$ in TSL, with some values as high as $-11‰$ (Table 1 and Fig. 3 *A* and *B*). Similar values were measured by Barbosa et al. (38) on Amazon River floodplains (δ^{13}C-$CH_4 = -70.1$ to $-14.8‰$). Independently measured rates of CH_4 production and oxidation in TSL support this conclusion. Both net CH_4 oxidation in the water column of TSL (Fig. 3 *B* and *C*) and gross CH_4 production within the sediments (Fig. 3 *D* and *E*) were strongly correlated to δ^{13}C-CO_2.

Despite these relationships, CH_4 production and oxidation and aerobic respiration within the water column and underlying sediments typically contribute less than 15% of dissolved CO_2 in TSL (*SI Appendix*, Table S4). In our mass balance, we solve for CO_2 advected from elsewhere, within inundated soils and other floodplain habitats, and infer that this is a far greater contributor to CO_2 supersaturation. This was initially hypothesized by Junk et al. (18) and later combined with the "active pipe" by Abril and Borges (20). Yet it has been empirically tested using dissolved CO_2 and CH_4 in only two other locations (15, 17) and never with the C isotopic composition of these dissolved gases.

The ^{13}C depletion of CO_2, ^{13}C enrichment of CH_4, and their correlations to independently measured rates of CH_4 production and oxidation suggest that these coupled processes support CO_2 supersaturation in TSL. By extension, coupled CH_4 production and oxidation are disproportionately responsible for CO_2 emissions from TSL. Lauerwald et al. (13) estimate that >50% of global riverine CO_2 emissions occur in the tropics, emphasizing the importance of tropical "active pipes." Data on the stable C isotopes of both CO_2 and CH_4 are rarely reported for freshwaters, though ^{13}C-enriched dissolved CH_4 ($>-50‰$) reported in tropical and temperate lakes, wetlands, peatlands, and the Amazon River implies widespread oxidation of CH_4 to CO_2 (*SI Appendix*, Table S5). Coupled CH_4 production and oxidation have thus been understudied but may support CO_2 supersaturation and CO_2 emissions from other tropical freshwaters with large amounts of seasonally or perennially flooded land. The extent of this flooding will most likely change under the twin stressors of hydropower development and climate change in the tropics (21), impacting the future role of floodplains in the transfer and transformation of C from terrestrial to aquatic ecosystems.

Materials and Methods

Field Sampling. Field sampling was conducted during the high-water and falling-water stages of the annual flood pulse in October 2015 and March 2016, respectively, representing the typical hydrological range in TSL. Flood stages were assessed using historical data from a gauging station at Kampong Luong (*SI Appendix*, Fig. S1) (21). Sampling focused on three locations in the southwest (Kampong Preah), central (Anlang Reang), and northwest (Prek Konteil) basins of TSL. Transects designed to capture horizontal gradients in dissolved O_2 and reducing conditions were established at each location. These transects consisted of six points extending through the distinct open water (Transect Point 1), edge (Transect Point 2), and floodplain environments of TSL (Transect Points 4 to 6). The edge environments were characterized by a transition from open water environments to emergent, permanently rooted floodplain vegetation.

Partial Pressures of CO_2 and CH_4. Partial pressures of CO_2 and CH_4 at each transect point and flood stage in TSL were quantified as the average of three duplicates collected at 0.1 m below the water surface and at 0.5 m above the lake bottom where water depth exceeded 0.5 m ($n = 143$ duplicates, $n = 47$ replicates). Water was collected into 74-mL gas-tight serum bottles using a van Dorn sampler, preserved in the field with 74 μL of 50% mass/volume zinc chloride solution, and placed on ice for transport to the Royal University of Phnom Penh, where they were stored at 4 °C until analysis. For analysis, samples were displaced with helium to roughly equal parts headspace and water, left to equilibrate for 12 h, and analyzed for headspace pCO_2 and pCH_4 using gas chromatography (SRI 8610*c* GC) by referencing to certified standards of known concentrations.

Stable C Isotopes of CO_2 and CH_4. Following analysis for partial pressures, samples were resealed with Apiezon grease, inverted, placed on ice, and transported to the University of Washington for C isotopic analysis ($n = 47$). A 20-mL headspace sample was analyzed for the $^{13}C/^{12}C$ of CO_2 and CH_4 simultaneously using a cavity ring-down spectrometer (Picarro G2201*i*) with a small sample introduction module (Picarro A0314 SSIM). Following Malowany et al. (39), a column of reduced copper shavings was installed on the small sample introduction module to eliminate interference by hydrogen sulfide with isotopic measurements. Samples exceeding 300 μatm CH_4 were diluted with ultra-high purity nitrogen to further eliminate interference by high concentrations of this gas with isotopic measurements. Stable C isotopes of CO_2 and CH_4 are each expressed in delta (δ) notation relative to Vienna Pee Dee Belemnite by referencing to certified CO_2 and CH_4 standards of known concentrations and $^{13}C/^{12}C$.

Stable C Isotopes of Organic and Inorganic C. Grab samples of floating macrophytes (*Eichhornia* species), terrestrial C3 vegetation, periphyton, and phytoplankton were collected across the distinct lake environments and flood stages of TSL, combined, and considered a single, lake-wide sample with a minimum of four replicates. Phytoplankton were collected using a Wisconsin net sampler (Wildco 40-A50), and periphyton was scraped from the benthos and the surfaces of floating macrophytes and emergent, aquatic vegetation. Macrophytes ($\delta^{13}C = -33 \pm 4‰$, $n = 4$), terrestrial C3 vegetation ($\delta^{13}C = -29 \pm 2‰$, $n = 7$), periphyton ($\delta^{13}C = -28 \pm 4‰$, $n = 18$), and phytoplankton ($\delta^{13}C = -24 \pm 4‰$, $n = 6$) in TSL were freeze dried, ground, and analyzed for bulk $^{13}C/^{12}C$ using an elemental analyzer (CE Instruments 2500 NA) interfaced with an isotope ratio mass spectrometer (DeltaV IRMS). Laboratory working standards were glutamic acid 1 ($\delta^{13}C = -28.3‰$ versus VPDB), glutamic acid 2 ($\delta^{13}C = -13.7‰$), and sockeye salmon ($\delta^{13}C = -21.3‰$). DIC ($\delta^{13}C = -13.8 \pm 0.4‰$, $n = 98$) samples from another sampling effort across the same lake environments and flood stages were acidified, displaced with a helium headspace, analyzed on a DeltaV IRMS, and considered a lake-wide sample, as described previously.

Depth-Integrated Gross Primary Production and Aerobic Respiration. Gross primary production (GPP) and aerobic respiration were modeled across the distinct lake environments and flood stages of TSL using diel-dissolved O_2 data in the "LakeMetabolizer" R package ($n = 16$) (40, 41). Model inputs include hourly dissolved oxygen (millimoles per liter), hourly water temperature (degrees Celsius), and hourly photon flux for photosynthetically active radiation (PAR; microeinsteins per second · per square meter). Continuously logging dissolved O_2 and water temperature sensors were deployed for a minimum of 20 h (Precision Measurement Engineering miniDO$_2$T Logger, accuracy $\pm$0.16 mg, O_2 L^{-1}, and $\pm$0.1 °C). Accuracy of dissolved O_2 sensors was verified prior to field deployment using the Winkler titration method. PAR was not measured directly but calculated from full-spectrum irradiance based on latitude, longitude, aspect, slope, transmissivity data, and the "astrocalc4r" function in the "fishmethods" R package (42). GPP and aerobic respiration were converted to millimoles of CO_2 per cubic meter per day using an assimilation efficiency of 1.2 for photosynthesis (43, 44) and a conversion efficiency of 1.0 for respiration.

Volumetric rates were multiplied by mixing depths to obtain areal rates in terms of millimoles of CO_2 per square meter per day. Mixing depths were evaluated with dissolved O_2 profiles at each site using a multiparameter sonde calibrated just prior to deployment with water-saturated air (YSI 6920). Dissolved O_2 data were plotted over depth (m), smoothed using a loess-spanning function of 0.2, and interrogated for inflection points in R (41). The depth of these inflection points at each transect was considered the mixing depth.

Depth-Integrated CH_4 Production and Oxidation. Gross CH_4 production within lake sediments was quantified as the average of three duplicate sediment incubations. At each transect point and flood stage in TSL, sediment cores were taken with a stainless-steel corer. The upper 1 cm^3 of each core was sealed inside a 74-mL gas-tight serum bottle ($n = 72$ duplicates, $n = 24$ replicates). The remaining volume of the bottle was filled with bottom water collected 0.5 m above the sediments. Three additional bottles were filled with bottom water only and three with water collected 0.1 m below the water surface. All bottles were incubated at ambient air temperatures (25 to 33 4 °C), which were typically <4 °C different from water temperatures in TSL and sampled daily from a helium headspace for 7 d. pCH_4 was analyzed as described previously and corrected for progressively decreasing headspace:water ratios. Net CH_4 oxidation in surface waters was multiplied by mixing depths to obtain areal rates as in *Depth Integrated Gross Primary Production and Aerobic Respiration*. Net oxidation in bottom waters was added to net CH_4 production measured in the bottles containing a combination of sediment cores and bottom water and considered gross CH_4 production. Following incubation, each sediment core was dried at 100 °C for 3 h and weighed. Gross CH_4 production rates were then corrected for sediment core weight and scaled to nanomoles of CH_4 per cubic meter per day. Previously published studies of CH_4 production in lake sediment cores show that rates measured at the sediment–water interface are consistent to a sediment depth of 0.1 m (25, 45). Volumetric rates of CH_4 production were thus multiplied by 0.1 m to obtain areal rates in terms of nanomoles of CH_4 per square meter per day. Because one mole of CO_2 is produced for each mole of CH_4 produced during acetate fermentation, presumed to be dominant in TSL (Fig. 2*B*) and within freshwaters more broadly (24, 25), rates were also considered in terms of nanomoles of CO_2 per square meter per day. Each transect sampled included negative control incubations amended with a 74 μ L of 50% mass/volume zinc chloride solution.

Mass Balance. A mass balance for dissolved CO_2 in TSL was created from processes resulting in a gain or loss of CO_2:

$$CO_{2,Measured} = CO_{2,Advected} + CO_{2,Respiration} - CO_{2,GPP} + CO_{2,MProd} + CO_{2,MOx},$$

where $CO_{2,Respiration}$ is the CO_2 gained from modeled aerobic respiration, $CO_{2,GPP}$ is the CO_2 lost from modeled GPP, $CO_{2,MProd}$ is the CO_2 gained from measured gross CH_4 production within sediments, and $CO_{2,MOx}$ is the CO_2 gained from measured net CH_4 oxidation in the water column, each in millimoles per square meter per day. $CO_{2,Measured}$ is the pCO_2 measured within the water column of TSL and multiplied by a temperature dependent Henry's constant and mixing depth to yield millimoles of dissolved CO_2 per square meter on the day of sampling. Diffusion of CO_2 from TSL to the atmosphere was modeled using $CO_{2,Measured}$ following Cole and Caraco (46). CO_2 diffusion reflects an atmospheric loss subsequent to $CO_{2,Measured}$ and was ultimately excluded from the mass balance. $CO_{2,Advected}$ is the remaining CO_2 in the mass balance assumed to result from aerobic respiration and anaerobic degradation of organic C elsewhere, within inundated soils and other floodplain habitats under steady-state conditions (millimoles per square meter per day). Mean daily $CO_{2,Advected} \pm 1$ SE was quantified using normal distributions—based on sample size, mean, and SD—of other terms in the mass balance over 10,000 Monte Carlo simulations in R (41).

Stable, Isotope-Mixing Model. The C isotopic composition of CO_2 measured in TSL fell between the $^{13}C/^{12}C$ produced by 1) the oxidation of ^{13}C-depleted CH_4 to CO_2 (−110 to −50‰) and 2) that of other potential organic and inorganic sources of CO_2 (−37 to −7.7‰). Here, the sole concern is the fraction of CO_2 derived from CH_4 oxidation. Thus, a two-source ("Methane" versus "Other"), stable, isotope-mixing model was deemed appropriate. The model also accounted for CO_2 losses from primary production and atmospheric diffusion and took the form:

$$\begin{aligned}\delta^{13}CO_2 = {} & \left(\delta^{13}C_{Methane} \cdot f_{Methane}\right) + \left(\delta^{13}C_{Other} \cdot f_{Other}\right) \\ & -\left(\left(\delta^{13}CO_{2,Measured} + \varepsilon_{GPP}\right) \cdot f_{GPP}\right) \\ & -\left(\left(\delta^{13}CO_{2,Measured} + \varepsilon_{Diffusion}\right) \cdot f_{Diffusion}\right)\end{aligned},$$

where $\Sigma f_i = 1.00$. $\delta^{13}C_{Methane}$ was modeled as a continuous, uniform distribution of $\delta^{13}C$-CH_4 values produced by methanogenesis, ranging from −110 to −50‰ (Fig. 2*A*) (24–26). $f_{Methane}$ is the fraction of CO_2 resulting from CH_4 oxidation. Because $\delta^{13}C_{Methane}$ encompasses the range of $\delta^{13}C$ values produced by both acetate fermentation (−65 to −50‰)—presumed to be dominant in TSL and within freshwaters more broadly (24, 25)—and carbonate reduction (−110 to −60‰), the model results in a conservative estimate of $f_{Methane}$ for this freshwater lake (Fig. 2*B*).

$\delta^{13}C_{Other}$ was also modeled as a continuous, uniform distribution of $\delta^{13}C$ values encompassing other potential sources of organic and inorganic C (*SI Appendix*, Fig. S2). This distribution ranges from the most ^{13}C-depleted source of organic C measured in TSL, macrophytes ($\delta^{13}C = -37$‰), to the most ^{13}C-enriched source of inorganic C, atmospheric CO_2 in equilibrium with water ($\delta^{13}C = -7.7$‰) (47). $\delta^{13}C_{Other}$ therefore encompasses the $\delta^{13}C$ of terrestrial C3 vegetation, periphyton, phytoplankton, and DIC measured in TSL and the $\delta^{13}C$ of emergent, aquatic C4 grasses ($\delta^{13}C = -12.2 \pm 0.3$‰) measured by Hedges et al. (48) in the Amazon. With multiple sources of organic and inorganic C that overlap in $\delta^{13}C$ and no prior information on the relative importance of each, the most parsimonious option was to treat them as a group with equal probability across the full range of $\delta^{13}C$ values. However, multiple alternative models were also tested (*SI Appendix*, Table S3).

$\delta^{13}C_{CO_{2,Measured}}$ and mass-dependent fractionations for photosynthesis (f_{GPP}) and diffusion to the atmosphere ($f_{Diffusion}$) in the model were quantified by this study and its mass balance (*SI Appendix*, Table S4). The kinetic fractionation factors for photosynthesis and diffusion, ε_{GPP} and $\varepsilon_{Diffusion}$, are −19 and −1.1‰, respectively (47). Following the IsoSource-mixing model by Phillips et al. (49), $f_{Methane}$ and f_{Other} were assigned possible values between 0.00 and 1.00 by 0.05, and was solved for iteratively in R (41). If the resulting $\delta^{13}CO_2 = \delta^{13}CO_{2,Measured} \pm 1$‰ and $f_{Other} > 0.15$ (allowing a minimum f_{Other} of 20%), then $f_{Methane}$ was saved. Sensitivities of the continuous, uniform distributions generated by the model were quantified over 10,000 Monte Carlo simulations in R (41). The mean of all saved $f_{Methane}$ values was then reported as the fraction of CO_2 resulting from CH_4 production and oxidation. Variance around these saved $f_{Methane}$ values is based on different, continuous uniform distributions generated at random by the mixing model and was ultimately not reported.

Statistical Analyses. Normality in the data were assessed using quantile–quantile plots and Shapiro–Wilk tests. Homogeneity of variance in the data were assessed using Levene's tests. pCH_4 and $\delta^{13}C$-CO_2 followed nonnormal distributions and were log transformed for parametric comparisons along with pCO_2 and $\delta^{13}C$-CH_4 across the distinct lake environments and flood stages of TSL using ANOVA. Multiple pairwise comparisons between means in the open water, edge, and floodplain environments during the high-water and falling-water stages were carried out subsequently using Tukey Honest Significant Differences. Our Bonferroni-corrected, critical alpha value for multiple pairwise comparisons was 0.025 (for linear regression, our critical alpha value remained 0.050). To assess whether differences between means were independent of sample size, we also calculated effect sizes using Cohen's *d*, where $d = 0.2$ to 0.4 corresponds to a small effect and low support for differences between means, $d = 0.5$ to 0.7 corresponds to a medium effect, and $d > 0.9$ corresponds to a large effect and high support for differences (50). All statistical analyses were conducted using R (41).

Data Availability. All data are freely available and can be accessed at the publically accessible repository GitHub, https://github.com/blm8/PNAS_Tonle-Sap-Carbon-Dioxide-Supersaturation. Code data have been deposited in GitHub, https://github.com/blm8/PNAS_Tonle-Sap-Carbon-Dioxide-Supersaturation. All other study data are included in the article and/or *SI Appendix*.

ACKNOWLEDGMENTS. We gratefully acknowledge assistance from the Cambodian Inland Fisheries Research and Development Institute, Cambodian Fisheries Administration, and inhabitants of the floating villages in TSL. We also thank Vittoria Elliott of World Fish and David Ford of Royal University of Phnom Penh for further in-country support. David Butman, Jeffrey Richey, Daniel Schindler, and two anonymous reviewers provided helpful comments during the preparation of this manuscript. This research was supported by the NSF and Margaret A. Cargill Foundation. B.L.M. was additionally supported by an NSF Graduate Research Fellowship and a National Security Education Program Boren Fellowship. M.E.A. was additionally supported by a Florida Education Fund McKnight Junior Faculty Fellowship. Portions of this paper were developed from the doctoral thesis of B.L.M.

1. J. J. Cole, N. F. Caraco, G. W. Kling, T. K. Kratz, Carbon dioxide supersaturation in the surface waters of lakes. *Science* **265**, 1568–1570 (1994).
2. P. A. Raymond *et al.*, Global carbon dioxide emissions from inland waters. *Nature* **503**, 355–359 (2013). Correction in: *Nature* **507**, 387 (2014).
3. G. W. Kling, G. W. Kipphut, M. C. Miller, Arctic lakes and streams as gas conduits to the atmosphere: Implications for tundra carbon budgets. *Science* **251**, 298–301 (1991).
4. J. E. Richey, A. H. Devol, S. C. Wofsy, R. Victoria, M. N. G. Riverio, Biogenic gases and the oxidation and reduction of carbon in Amazon River and floodplain waters. *Limnol. Oceanogr.* **33**, 551–561 (1988).
5. J. B. Jones Jr., P. J. Mulholland, Carbon dioxide variation in a hardwood forest stream—An integrative measure of whole catchment soil respiration. *Ecosystems* **1**, 183–196 (1998).

6. P. A. Raymond, J. E. Saiers, W. V. Sobczak, Hydrological and biogeochemical controls on watershed dissolved organic matter transport: Pulse-shunt concept. *Ecology* **97**, 5–16 (2016).
7. P. Lopez, R. Marce, J. Armengol, Net heterotrophy and CO_2 evasion from a productive calcareous reservoir—Adding complexity to the metabolism-CO_2 evasion issue. *J. Geophys. Res.* **116**, G02021 (2011).
8. R. Marce *et al.*, Carbonate weathering as a driver of CO_2 supersaturation in lakes. *Nat. Geosci.* **8**, 107–111 (2015).
9. P. A. Del Giorgio, J. J. Cole, N. F. Caraco, R. H. Peters, Linking planktonic biomass and metbolism to net gas fluxes in northern temperate lakes. *Ecology* **80**, 1422–1431 (1999).
10. J. J. Cole, N. F. Caracao, Carbon in catchments—Connecting terrestrial carbon losses with aquatic metabolism. *Mar. Freshw. Res.* **52**, 101–110 (2001).
11. J. J. Cole *et al.*, Plumbing the global carbon cycle—Integrating inland waters into the terrestrial carbon budget. *Ecosystems* **10**, 171–185 (2007).
12. R. Lauerwald, G. G. Laruelle, J. Hartmann, P. Ciais, P. A. G. Regnier, Spatial patterns in CO2 evasion from the global river network. *Global Biogeochem. Cycles* **29**, 534–554 (2015).
13. J. E. Richey, J. M. Melack, A. K. Aufdenkampe, V. M. Ballester, L. L. Hess, Outgassing from Amazonian rivers and wetlands as a large tropical source of atmospheric CO2. *Nature* **416**, 617–620 (2002).
14. G. Abril *et al.*, Amazon River carbon dioxide outgassing fuelled by wetlands. *Nature* **505**, 395–398 (2014).
15. J. H. F. Amaral *et al.*, Seasonal and spatial variability of CO_2 in aquatic environments of the central lowland Amazon basin. *Biogeochemistry* **143**, 133–149 (2019).
16. W. J. Junk, P. B. Bayley, R. E. Sparks, "The flood pulse concept in river-floodplain systems" in *Proceedings of the International Large River Symposium*, D. P. Dodge, Ed. (Canadian Special Publication of Fisheries and Aquatic Sciences, Ottawa, Canada, 1989), pp. 110–127.
17. A. Zuijdgeest, S. Baumgartner, B. Wehrli, Hysteresis effects in organic matter turnover in a tropical floodplain during a flood cycle. *Biogeochemistry* **131**, 49–63 (2016).
18. A. V. Borges *et al.*, Divergent biophysical controls of aquatic CO2 and CH4 in the World's two largest rivers. *Sci. Rep.* **5**, 15614 (2015).
19. G. Abril, A. V. Borges, Ideas and perspectives—Carbon leaks from flooded land—Do we need to replumb the inland water active pipe? *Biogeosciences* **16**, 769–784 (2019).
20. M. E. Arias *et al.*, Quantifying changes in flooding and habitats in the Tonle Sap Lake (Cambodia) caused by water infrastructure development and climate change in the Mekong Basin. *J. Environ. Manage.* **112**, 53–66 (2012).
21. G. W. Holtgrieve *et al.*, Patterns of ecosystem metabolism in the Tonle Sap Lake, Cambodia with links to capture fisheries. *PLoS One* **8**, e71395 (2013).
22. A. V. Borges *et al.*, Variations in dissolved greenhouse gases (CO_2, CH_4, N_2O) in the Congo River overwhelmingly driven by fluvial wetland connectivity. *Biogeosciences* **16**, 3801–3834 (2019).
23. S. K. Hamilton, S. J. Sippel, D. F. Calheiros, J. M. Melack, An anoxic event and other biogeochemical effects of the Pantanal wetland on the Paraguay River. *Limnol. Oceanogr.* **42**, 257–272 (1997).
24. M. J. Whiticar, E. Faber, Methane oxidation in sediment and water column environments—Isotopic evidence. *Org. Geochem.* **10**, 759–768 (1986).
25. M. J. Whiticar, Carbon and hydrogen isotope systematics of bacterial formation and oxidation of methane. *Chem. Geol.* **161**, 291–314 (1999).
26. E. R. Hornibrook, F. J. Longstaffe, W. S. Fyfe, Evolution of stable C isotope compositions for methane and carbon dioxidein freshwater wetlands and other anaerobic environments. *Geochim. Cosmochim. Acta* **64**, 1013–1027 (2000).
27. W. Burnett *et al.*, Groundwater discharge and phosphorus dynamics in a flood-pulse system—Tonle Sap Lake, Cambodia. *J. Hydrol.* **549**, 79–91 (2017).
28. C. D. Keeling, The concentration and isotopic abundance of carbon dioxide in rural areas. *Geochim. Cosmochim. Acta* **13**, 322–334 (1958).
29. C. D. Keeling, The concentration and isotopic abundance of carbon dioxide in rural and marine air. *Geochim. Cosmochim. Acta* **24**, 277–298 (1961).
30. A. Dai, K. E. Trenberth, Estimates of freshwater discharge from continents—Latitudinal and seasonal variations. *J. Hydrometeorol.* **3**, 660–687 (2002).
31. J.-F. Pekel, A. Cottam, N. Gorelick, A. S. Belward, High-resolution mapping of global surface water and its long-term changes. *Nature* **540**, 418–422 (2016).
32. B. J. Peterson, B. Fry, Stable isotopes in ecosystem studies. *Annu. Rev. Ecol. Syst.* **18**, 293–320 (1987).
33. A. De Kluijver, P. L. Schoon, J. A. Downing, S. Schouten, J. J. Middleburg, Stable carbon isotope biogeochemistry of lakes along a trophic gradient. *Biogeosciences* **11**, 6265–6276 (2014).
34. S. L. McCallister, P. A. Del Giorgio, Direct measurement of the d13C signature of carbon respirared by bacteria in lakes—Linkages to potential carbon sources, ecosystem baseline metabolism, and CO2 fluxes. *Limnol. Oceanogr.* **53**, 1204–1216 (2008).
35. J. M. Melack, D. L. Engle, An organic carbon budget for an Amazon floodplain lake. *Verh. Int. Ver. Theor. Angew. Limnol.* **30**, 1179–1182 (2009).
36. R. Conrad, M. Klose, P. Claus, A. Enrich-Prast, Methanogenic pathway, 13C isotope fractionation, and archaeal community composition in the sediment of two clear-water lakes of Amazonia. *Limnol. Oceanogr.* **55**, 689–702 (2010).
37. R. Conrad *et al.*, Stable carbon isotope discrimination and microbiology of methane formation in tropical anoxic lake sediments. *Biogeosciences* **8**, 795–814 (2011).
38. P. M. Barbosa *et al.*, High rates of methane oxidation in an Amazon floodplain lake. *Biogeochemistry* **137**, 351–365 (2018).
39. K. Malowany, J. Stix, A. Ven Pelt, G. Luic, H2S interference on CO_2 isotopic measurements using a Picarro G1101-i cavity ring-down spectrometer. *Atmos. Meas. Tech.* **8**, 5651–5675 (2015).
40. L. A. Winslow *et al.*, LakeMetabolizer—An R package for estimating lake metabolism from free-water oxygen using diverse statistical models. *Inland Waters* **6**, 622–636 (2016).
41. R Core Team, R—A Language and Environment for Statistical Computing (Version 4.1.0, R Foundation for Statistical Computing, Vienna, Austria, 2019).
42. G. A. Nelson, fishmethods—Fishery science methods and models (R package Version 1.11-1, 2019). https://cran.r-project.org/web/packages/fishmethods/index.html. Accessed 1 May 2020.
43. G. E. Likens, "Primary production of inland aquatic ecosystems" in *Primary Productivity of the Biosphere*, H. Leith, R. H. Whittaker, Eds. (Springer, 1975), pp. 185–202.
44. J. M. Melack, Primary productivity and fish yields in tropical lakes. *Trans. Am. Fish. Soc.* **105**, 575–580 (1976).
45. B. Thebrath, F. Rothfuss, M. J. Whiticar, R. Conrad, Methane production in littoral sediment of Lake Constance. *FEMS Microbiol. Lett.* **11**, 279–289 (1993).
46. J. J. Cole, N. F. Caraco, Atmospheric exchange of carbon dioxide in a low wind oligotrophic lake measured by the addition of SF6. *Limnol. Oceanogr.* **43**, 647–656 (1998).
47. M. H. O'Leary, Carbon isotope fractionation in plants. *Phytochemistry* **20**, 553–567 (1981).
48. J. I. Hedges W. A. Clark, P. D. Quay, J. E. Richey, A. H. Devol, Compositions and fluxes of particulate organic material in the Amazon River. *Limnol. Oceanogr.* **31**, 717–738 (1986).
49. D. L. Phillips, S. D. Newsome, J. W. Gregg, Combining sources in stable isotope mixing models: Alternative methods. *Oecologia* **144**, 520–527 (2005).
50. J. Cohen, *Statistical Power Analysis for the Behavioral Sciences* (Lawrence Earlbaum Associates, 1988).